IOP Publishing Plasma Physics and Controlled Fusion
Plasma Phys. Control. Fusion **61** (2019) 035012 (13pp) https://doi.org/10.1088/1361-6587/aaf94b

Highly collimated electron acceleration by longitudinal laser fields in a hollow-core target

Z Gong[1,2], A P L Robinson[3], X Q Yan[1] and A V Arefiev[4,5]

[1] State Key Laboratory of Nuclear Physics and Technology, and Key Laboratory of HEDP of the Ministry of Education, CAPT, Peking University, Beijing 100871, People's Republic of China
[2] Center for High Energy Density Science, The University of Texas, Austin, TX 78712, United States of America
[3] Central Laser Facility, STFC Rutherford-Appleton Laboratory, Didcot OX11 0QX, United Kingdom
[4] Department of Mechanical and Aerospace Engineering, University of California at San Diego, La Jolla, CA 92093, United States of America

E-mail: alex.robinson@stfc.ac.uk, x.yan@pku.edu.cn and aarefiev@eng.ucsd.edu

Received 24 October 2018, revised 12 November 2018
Accepted for publication 13 December 2018
Published 7 February 2019

Abstract

The substantial angular divergence of electron beams produced by direct laser acceleration (DLA) is often considered as an inherent negative feature of the mechanism. The divergence however arises primarily because the standard approach relies on transverse electron oscillations and their interplay with the transverse electric fields of the laser pulse. We consider a conceptually different approach to DLA that leverages longitudinal laser electric fields that are present in a tightly focused laser beam. A structured hollow-core target is used to enhance the longitudinal fields and maintain them over a distance much longer than the Rayleigh length by guiding the laser pulse. Electrons are injected by the transverse laser electric field into the channel and then they are accelerated forward by the pulse, generating an electron current. We show that the forces from electric and magnetic fields of this electron population compensate each other, creating a favorable configuration without a strong restoring force. We use two-dimensional particle-in-cell simulations to demonstrate that a low divergence energetic electron beam with an opening angle of less than 5° can be generated in this configuration. Most of the energy is transferred to the electrons by the longitudinal laser electric field and, given a sufficient acceleration distance, super-ponderomotive energies can be realized without sacrificing the collimation.

Keywords: laser-plasma interaction, high-intensity laser, electron acceleration

(Some figures may appear in colour only in the online journal)

1. Introduction

The development of relativistically intense laser pulses [1–3] has enabled several schemes for producing laser-driven relativistic electron bunches. One such scheme is direct laser acceleration (DLA) [4, 5]. The normalized amplitude of the electric field in a laser pulse with wavelength λ and intensity I_0 is defined as $a_0 \equiv \sqrt{I_0(\mathrm{W\,cm^{-2}})/1.37 \times 10^{18}}\,\lambda(\mu\mathrm{m})$. If I_0 exceeds 1.37×10^{18} W cm^{-2}, then this implies that the work done by the laser field during one period is comparable with the electron rest energy. As the electron velocity is boosted close to the speed of light in one laser cycle, the electron also gains considerable momentum in the direction of laser propagation via the Lorentz force, i.e. the $\mathbf{v} \times \mathbf{B}$ term in the equation of motion. If the electron were to maintain its relative phase with respect to the laser field then this longitudinal momentum $p_\parallel$ would become very large [6]. However, even in the case of an infinite plane wave, the natural relativistic dephasing rate limits this to $p_\parallel/m_e c = a_0^2/2$, where m_e is the electron mass and c is the speed of light. In reality, the

[5] Author to whom any correspondence should be addressed.

momentum may be even more limited due to diffraction of the laser pulse [7–9], which raises questions about the limits of what can be achieved with DLA.

A conventional approach to DLA is to employ a uniform plasma slab that not only restrains the laser defocusing [10, 11] but also maintains a plasma channel with a positively charged and slowly evolving ion background [4, 12]. The ions generate a transverse electric field that confines laser-accelerated electrons inside the channel, preventing them from being prematurely expelled by the transverse ponderomotive force of the laser pulse. The ion electric field forces the accelerated electrons towards the axis of the channel and the ensuing transverse oscillations can be successfully leveraged to enhance the electron energy gain from the laser pulse [13–15]. Even though a dense energetic electron bunch can be generated using this approach [16, 17], the bunch unavoidably has a relatively large divergence angle that can exceed 20° due to the transverse oscillations. Such significant divergence that is also difficult to control might be undesirable for some potential applications. For example, the photon emission by the DLA electron bunch [18–23] inherits the angular divergence which then impacts the brilliance of the resulting advanced light sources.

It has been recently shown that structured targets can have a significant benefit if the end-goal is to generate a large number of energetic electrons in the form of a collimated beam [24, 25]. For example, a microwire array attached to a solid density target can be used to guide the irradiating laser pulse and to provide a reliable source of electrons that can then be accelerated to high energies. In the case of a flat solid-density target, the electrons usually come from a pre-plasma whose characteristics are determined by the laser pre-pulse. As a result, experimentally observed electron acceleration is difficult to control and to predict using numerical simulations. A structured target, as the one considered in [24, 25], provides the much needed control over the electron acceleration. It has been shown using numerical simulations that longitudinal electric fields can have a significant impact on electron acceleration in this setup [26]. Similar tailored tube targets have also been considered for the purpose of generating attosecond electron bunches [27] and enhancing laser-driven ion acceleration [28, 29].

Here, we continue the research of laser-irradiated structured targets by considering a hollow-core target whose channel width is smaller than the width of the irradiating laser beam. We report a new scheme for achieving a collimated laser-accelerated energetic electron bunch that utilizes longitudinal laser electric fields. By focusing a relativistically intense laser pulse into a hollow-core target, an electron channel, only filled with negative charge, can be produced in the hollow region. We demonstrate that, in contrast to the fields in the ion channel [12], quasi-static electric and magnetic fields induce transverse forces that nearly compensate each other for forward-moving ultra-relativistic electrons. This provides an avenue to eliminate the transverse oscillations and reduce the angular divergence of the accelerated electrons. Moreover, the reduction of the transverse oscillations greatly facilitates electron acceleration by the longitudinal laser electric field, since the electrons can now remain in the favorable phase of the wave for much longer. Combined with the strengthened longitudinal laser field, a collimated longitudinal laser field acceleration is realized.

The paper is organized as follows: in sections 2 and 3, we show how the hollow-core target can produce the favorable channel fields. In section 4, the acceleration mechanism is demonstrated by tracking the accelerated electrons and the work performed by transverse and longitudinal laser electric fields. In section 5, we show that the electrons accelerated by the longitudinal field can be highly collimated and that their energy can significantly exceed what is achievable in a pure vacuum case. In section 6, the key conclusions of this work are summarized. The details of the setup used in the simulations are given in the appendix A.

2. Enhancement of the longitudinal laser field by a hollow channel

Efficient acceleration via DLA requires that the laser pulse propagates in a stable fashion for a sufficiently long distance. Since we must, in reality, utilize focused laser pulses, the defocussing of the laser pulse, via diffraction, puts a fundamental limit on the longitudinal spatial range over which a given intensity can be maintained. In the case of a Gaussian beam, this length is given by the Rayleigh length $l_R = \pi\sigma_0^2/\lambda$, where σ_0 is the beam waist in the focal plane and λ is the laser wavelength. The transverse electric field of a beam propagating along the x-axis scales as

$$E_\perp^{3D} \propto \frac{\sigma_0}{\sigma(x)} \exp\left(-\frac{r^2}{\sigma^2(x)}\right), \tag{1}$$

where r is the radial distance from the beam axis and

$$\sigma(x) = \sigma_0\sqrt{1 + (x - x_0)^2/l_R^2}. \tag{2}$$

The focal plane is located at $x = x_0$, so the beam radius is increased by a factor of $\sqrt{2}$ and the corresponding beam cross sectional area by a factor of 2 at $x = x_0 + l_R$. Therefore, the beam on-axis intensity at a Rayleigh length away from the beam waist is less by a factor of 2 than the peak intensity at the beam waist. If the Gaussian beam is two-dimensional (2D), as in the simulations that we present in this paper, then

$$E_y^{2D} \propto \sqrt{\frac{\sigma_0}{\sigma(x)}} \exp\left(-\frac{y^2}{\sigma^2(x)}\right), \tag{3}$$

where y is the non-ignorable transverse coordinate. The on-axis intensity then decreases as $\sigma_0/\sigma(x)$ away from the beam waist due to the reduced dimensionality.

In order to demonstrate how a hollow channel can mitigate the diffraction, we have compared two 2D simulations. The 'control' simulation considers only a 2D Gaussian beam, where a laser pulse with a peak intensity of $I_0 = 5.4 \times 10^{20}$ W cm^{-2}, corresponding to $a_0 \approx 20$, propagates in vacuum. The other beam parameters are $\sigma_0 = 4$ μm, $\lambda = 1$ μm, and $x_0 = 5$ μm. The result in figure 1(a) shows that the beam width expands to $\sigma \approx 8.9$ μm by $x = 100$ μm, which is in good agreement with equation (2). The longitudinal laser field E_x must satisfy the

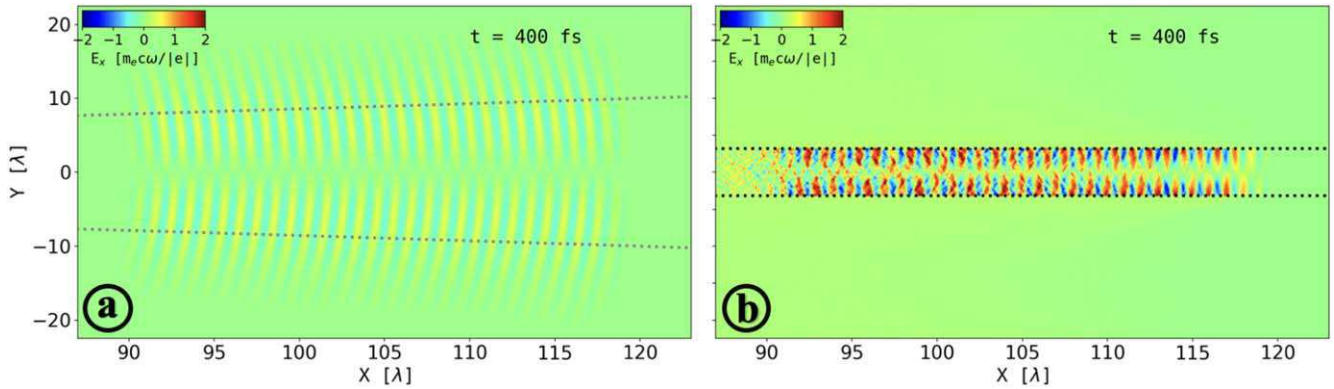

Figure 1. Structure of the longitudinal electric field E_x generated by a 2D Gaussian pulse in a vacuum (a) and inside a hollow-core target (b). In both cases, the focal plane is located at $x = 5$ μm, which is also the location of the target boundary in (b). The dotted curve in (a) marks the beam width $\sigma(x)$ given by equation (2). The dotted line in (b) marks the initial boundary of the hollow-core.

condition $\nabla \cdot E = 0$, which readily gives the following estimate for its maximum amplitude:

$$|E_x|_{\max} \approx \frac{\lambda}{2\pi} \left| \frac{\partial E_y}{\partial y} \right|_{\max} \sim \frac{\lambda}{\sigma(x)} \sqrt{\frac{\sigma_0}{\sigma(x)}} E_0, \qquad (4)$$

where E_0 is amplitude of the transverse field in the focal plane located at $x = x_0$. The longitudinal field peaks away from the beam axis at $y = \sigma(x)/\sqrt{2}$, which can be shown using equations (3) and (4). We find that at $x = 100$ μm the longitudinal field is already only $|E_x|_{\max} \approx 10^{-2} E_0$. Such a low longitudinal field is unlikely to provide efficient longitudinal acceleration (LDA).

In the second simulation, a hollow-core target with an inner radius of $r_d = 3.2$ μm and an electron density of $n_e = 50 n_c$ is utilized to optically guide the laser pulse. Here $n_c \equiv m_e \omega^2 / 4\pi e^2$ is the classical critical density that determines the density cutoff for propagation of laser pulses with $a_0 < 1$, where ω is the frequency of the laser pulse and e is the electron charge. The electron density cutoff increases to roughly $a_0 n_c$ for laser pulses with $a_0 \gg 1$ due to the relativistically induced transparency. Our target remains opaque to the laser pulse, since $n_e = 50 n_c > a_0 n_c \approx 20 n_c$. The simulation result in figure 1(b) shows the advantages of using the hollow-core channel: not only does the structured target suppress the transverse diffraction of the laser pulse, but also the laser longitudinal field is enhanced. The beam width is now limited to be less than $r_d = 3.2$ μm. Already at $x = 100$ μm it is substantially smaller than the beam width in the vacuum case that is determined by the diffraction, with $\sigma \approx 9$ μm. Moreover, the transverse profile of E_y is now more similar to a super-Gaussian function, with $E_y \propto \exp(-y^\kappa/\sigma^\kappa)$. This leads to the longitudinal laser field being enhanced by an additional factor of κ compared the longitudinal field in a Gaussian pulse of the same width. Figure 1(b) shows that the amplitude of the longitudinal electric field in the hollow-core target is $E_x \approx 0.1 E_0$, which is ten times bigger than E_x in the vacuum case at $x = 100$ μm. The observed sustained enhancement of the longitudinal laser field would play a significant role in electron acceleration.

It is worth emphasizing that the reason for the observed enhancement of E_x is the reduced transverse size of the hollow-core relative to the focal spot of the incoming laser pulse. We have compared longitudinal line-outs of the transverse laser electric field at two different times with the envelope of the incoming laser pulse in the vicinity of the focal plane. We found no significant enhancement of E_y and, in fact, it is reduced as the pulse propagates further into the target. Even though the Fresnel-like diffraction has been known to increase the laser field in structured targets [30], this effect is insignificant in the regime considered here.

3. Quasi-static field structure inside the hollow channel

In addition to the laser fields, there are also fields that are generated by the target itself in response to the laser pulse. The total force induced by these fields on the laser-accelerated electrons is dramatically different in the channel of a hollow-core target as compared to the force in a channel produced in an initially uniform target.

We first review the field structure in the ion channel that features in the 'standard' approach to DLA. In an initially uniform target, the laser beam tends to expel some electrons radially outwards, creating a positively charged channel. The corresponding transverse quasi-static electric field is directed away from the axis and, in the 2D case, it is roughly given by

$$\frac{|e|\overline{E}_y}{m_e \omega c} \approx \frac{\Delta n_i}{n_c} \frac{y\omega}{c}, \qquad (5)$$

where Δn_i is the uncompensated ion density that we assume to be constant across the channel. At the same time, the electrons that are present in the channel are pushed forward by the laser pulse, creating a longitudinal current. In the 2D case, the corresponding quasi-static magnetic field is directed along the z-axis and it is given by

$$\frac{|e|\overline{B}_z}{m_e \omega c} \approx -\frac{|j_x|}{|e| n_c c} \frac{y\omega}{c}, \qquad (6)$$

where $j_x < 0$ is the electron current density that, for simplicity, we assume to be constant and negative (because of the forward motion) across the channel. The transverse force induced by these electric and magnetic fields on a forward

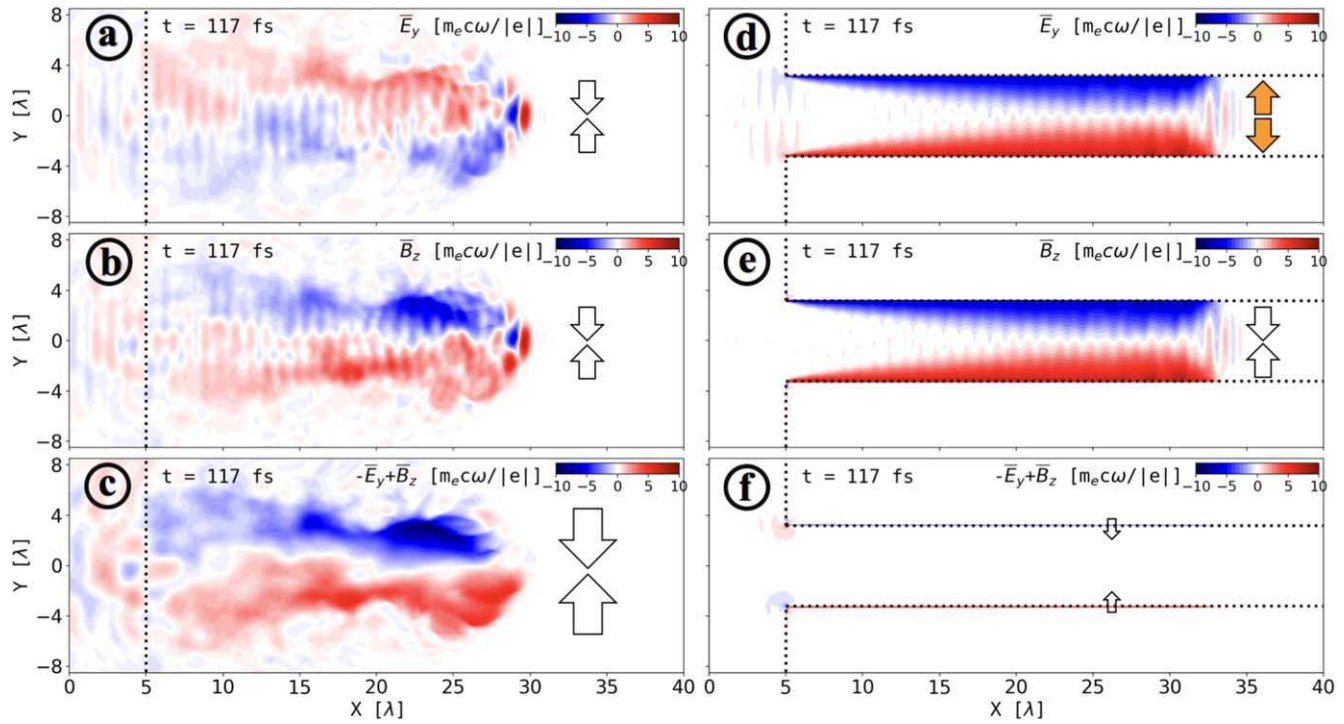

Figure 2. Structure of the quasi-static electric (a) and (d) and magnetic fields (b) and (e) in an initially uniform (left) and in a hollow-core target (right). The fields are calculated by time-averaging over one laser period. The lower two panels (c) and (f) show the total force exerted on an ultra-relativistic forward-moving electron, $v_x \to c$. In each panel, arrows indicate the direction of a transverse force exerted on a forward-moving electron.

moving electron in the ion channel is always directed towards the axis:

$$F_y^{\mathrm{IC}} = -|e|\left(\overline{E}_y - \frac{v_x}{c}\overline{B}_z\right) \approx -m_e\omega c\left(\frac{\Delta n_i}{n_c} + \frac{v_x}{c}\frac{|j_x|}{|e|n_c c}\right)\frac{y\omega}{c} \leqslant 0. \quad (7)$$

Equation (7) illustrates a well-known result that the quasi-static plasma fields in a uniform target generate a restoring force for forward moving laser-accelerated electrons that pushes them towards the axis of the channel. We have performed a 2D PIC simulation for a uniform target with an initially uniform electron density of $n_e = 0.5n_c$ irradiated by the laser pulse shown in figure 1(a). Quasi-static electric and magnetic fields are calculated by averaging the fields in the simulation over one laser period, with the corresponding time-averaged values denoted using an overhead bar. The profiles of $\overline{E}_y$ and $\overline{B}_z$, shown in figures 2(a) and (b), qualitatively agree with our estimates: $\overline{E}_y > 0$ and $\overline{B}_z < 0$ above the axis for $y > 0$, whereas $\overline{E}_y < 0$ and $\overline{B}_z > 0$ below the axis for $y < 0$. The combined transverse force induced by these fields and shown in figure 2(c) for an electron with $v_x \approx c$ is indeed directed towards the axis of the laser-produced channel.

In contrast to the uniform target, there are initially no particles inside the channel of the hollow-core target, which leads to a very different electric field structure. This region is populated with electrons as a result of the laser pulse interaction with the channel walls. As shown in figure 3(a), the electrons are ripped out of the wall by E_y of the laser pulse. Once the injected electrons fill up the channel, the quasi-static electric field is roughly given by

$$\frac{|e|\overline{E}_y}{m_e\omega c} \approx -\frac{\Delta n_e}{n_c}\frac{y\omega}{c}, \quad (8)$$

where n_e is the electron density. This field, shown in figure 2(d), is directed away from the axis, so it is opposite to the field of the ion channel, shown in figure 2(a) and estimated by equation (5). The magnetic field, however, is generated via exactly the same mechanism as in the ion channel and it can again be estimated using equation (6). This corresponding field structure is shown in figure 2(e). It is convenient to express the electron current density explicitly in terms of n_e: $j_x = -|e|n_e u$, where u is the effective velocity of the electron population in the channel. The total transverse force induced by the quasi-static electric and magnetic fields on a forward moving electron in the hollow-core target is then given by:

$$F_y^{\mathrm{HC}} = -|e|\left(\overline{E}_y - \frac{v_x}{c}\overline{B}_z\right) \approx m_e\omega c\frac{n_e}{n_c}\left(1 - \frac{uv_x}{c^2}\right)\frac{y\omega}{c} \geqslant 0. \quad (9)$$

A comparison of equations (7) and (9) confirms that the change in the direction of the quasi-static electric field in the hollow-core target qualitatively alters the total transverse force exerted on laser-accelerated electrons. The total force for a forward moving electron is now expelling, $F_y^{\mathrm{HC}} \geqslant 0$, instead of confining, $F_y^{\mathrm{IC}} \leqslant 0$. More importantly, the forces

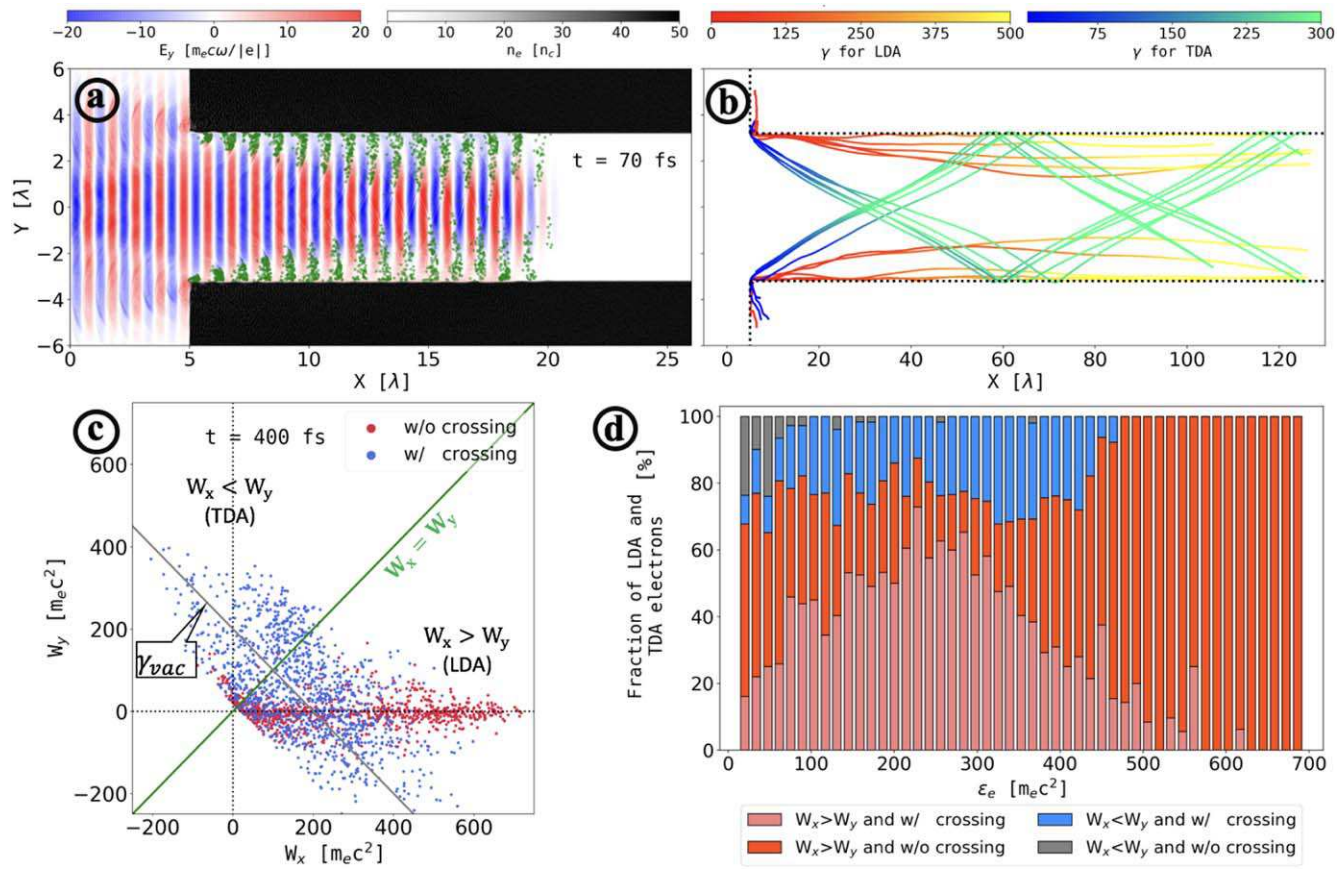

Figure 3. Electron injection and acceleration in a hollow-core target. (a) The transverse electric field E_y is plotted on top of the electron density n_e, while the injected electrons are shown by green dots. (b) Representative trajectories of laser-accelerated electrons are plotted over 400 fs. The γ-factor for LDA and TDA electrons is shown with the red-yellow and blue-green color-schemes. (c) The work performed by E_x and E_y on each of 2000 randomly selected injected electron over 400 fs is presented as a scatter-plot, where the color indicates whether the electron crossed the axis (blue) or not (red). (d) The relative fraction of LDA and TDA electrons from panel (c) is shown as a function of final energy (at $t = 400$ fs). Additional color-coding for each group indicates how many electrons have crossed the axis and how many have not.

induced by the electric and magnetic fields compensate each other with the compensation becoming significant for ultra-relativistic forward-moving electrons ($v_x \to c$) and a relativistic electron current ($u \to c$). The compensation is evident from figures 2(c) and (f), where the forces are calculated for an ultra-relativistic forward moving electron with $v_x \to c$. Even though the amplitudes of the electric, $|\overline{E}_y|$, and magnetic, $|\overline{B}_z|$, fields are higher in the hollow-core target (figures 2(d) and (e)) than in the ion channel (figures 2(a) and (b)), the total transverse force is drastically reduced, $|F_y^{HC}| \ll |F_y^{IC}|$.

It is important to point out that there are narrow regions at the wall of the channel where some uncompensated force is still present. These regions, associated with uncompensated ion charge, are aligned along the horizontal dotted lines in figure 2(f) that mark the initial boundary of the hollow-core. The force is instrumental in preventing laser-accelerated electrons from sliding out of the hollow channel. As we show in the next section of the paper, the combination of the enhanced longitudinal laser field E_x and the reduction of the strong restoring force F_y creates the conditions necessary for collimated longitudinal electron acceleration.

4. Longitudinal and transverse electron acceleration in the channel

The transverse restoring force exerted on laser-accelerated electrons in the ion channel and shown in figure 2(c) causes transverse electron oscillations across the channel that can be successfully leveraged to enhance the electron energy gain from the laser pulse [13–15]. The energetic electron bunch generated using this approach [16, 17] has a considerable divergence angle that is unavoidable. In this scenario that has become synonymous with DLA, the energy is transferred from the transverse laser electric field to the transverse electron motion and only then the strong laser magnetic field converts it into the kinetic energy of the forward-directed motion. The energy transfer is then the work performed by E_y:

$$W_y = -\int |e| E_y v_y \mathrm{d}t. \tag{10}$$

There is almost no net energy gain from the quasi-static plasma field $|\overline{E}_y|$ in each transverse oscillation across the channel and the vast majority of the energy comes from the oscillating laser field. In the case of an ultra-relativistic

electron, we have $E_y v_y \approx E_y c \sin\theta$, where θ is the angle between the electron velocity and the axis of the channel. Evidently, it is impossible to significantly decrease the divergence, which would be equivalent to decreasing the angle θ, without effectively halting the energy transfer and thus the conventional DLA process.

Electron acceleration by longitudinal laser electric fields offers a conceptually different path for achieving large electron energies that circumvents the described difficulty. In this case, the work performed by the laser pulse goes directly towards increasing the energy of the longitudinal electron motion

$$W_x = -\int |e| E_x v_x \mathrm{d}t, \tag{11}$$

without the need for the transverse oscillations to mediate the process. Even though the advantage of this approach is well recognized, there are several obstacles that have prevented its direct implementation. The approach requires a strong longitudinal laser electric field, but that can only be achieved if the laser pulse is tightly focused, as evident from equation (4). However, a tightly focused laser pulse has a short Rayleigh length, which limits the length over which an electron can be accelerated in a vacuum. Additionally, there is a significant transverse ponderomotive force in such a pulse, so the electron is quickly expelled radially outwards as the laser intensity ramps up. As a result, the electron might not even experience the peak intensity and there is also a possibility that it might be expelled before it reaches the focal region with a strong longitudinal electric field while moving forward.

The hollow-core target removes the obstacles that exist in the case of pure vacuum acceleration and thus enables effective acceleration by the longitudinal electric field. We have already demonstrated in section 2 that the longitudinal laser electric field E_x can be enhanced and maintained at that level over distances that greatly exceed the Rayleigh length. The electrons accelerated inside the channel of the hollow-core target originate from the peripheral wall region. They are extracted from the wall and injected into the channel by the transverse laser electric field E_y at the channel entrance, as shown in figure 3(a). It is critical that these electrons are injected immediately into a strong laser field. The transverse expelling ponderomotove force is approximately given by [13]

$$F_y \approx -\frac{1}{\gamma}\frac{\partial a_0^2}{\partial y} m_e c^2, \tag{12}$$

where $\gamma \equiv 1/\sqrt{1 - v^2/c^2}$ is the relativistic factor. Since $F_y \propto 1/\gamma$, its role is quickly reduced as the electrons become ultra-relativistic in the strong laser field and this is the reason why the injected electrons are not easily expelled.

The electron extraction can only take place if E_y is pointing into the wall of the channel. This is why the extraction location alternates between the upper and the lower channel walls. Figure 3(a) clearly illustrates this periodicity, with the injected electron bunches at the lower wall being shifted by half a laser cycle relative to the electron bunches injected at the upper wall. In order to generate the plot of the injected electrons, we first randomly selected 4% of the electrons in the simulation and then those with $\gamma > 1.5$ and $|y| < 3.2$ μm were plotted with green dots. The charge and current of the injected electrons sustain the channel electric and magnetic fields shown in figures 2(d) and (e). It is worth pointing out that these are ultra-relativistic electrons with a predominantly longitudinal velocity, so the effective velocity u that determines the electron current is very close to the speed of light. As discussed in section 3, this leads to the significant reduction of the transverse force given by equation (9) and shown in figure 2(f).

Our focus is the role of the LDA in achieving high electron energies, so we divide electrons based on the amount of work performed by longitudinal and transverse electric fields into two groups to aid our analysis:

- Group #1 with $W_x > W_y$: The longitudinal field E_x does more work on these electrons than the transverse field E_y. For compactness, we call this group LDA, which stands for longitudinal dominant acceleration.
- Group #2 with $W_x \leqslant W_y$: The work by the longitudinal field E_x does not exceed that of the transverse field E_y. For compactness, we call this group TDA, which stands for transverse dominant acceleration.

Figure 3(c) shows how the total work is partitioned between W_x and W_y for the injected electrons at $t = 400$ fs, where each dot represents a macro-particle. The dots below the solid green line are LDA electrons. The plot was generated by randomly selecting 2000 injected electrons with $|y| < 3.2$ μm.

Figure 3(d) shows the relative fraction of LDA electrons as a function of energy. A significant portion of the electrons in figure 3(d) are LDA electrons regardless of the energy, which confirms that the longitudinal laser electric field indeed plays a major role in electron acceleration. It is remarkable that an appreciable fraction of the injected electrons are very energetic at this stage, as their energy exceeds the so-called vacuum limit $\varepsilon_{\mathrm{vac}}$ for an electron in a plane wave. These are the electrons above the gray line in figure 3(c). The vacuum limit is the maximum energy for an initially immobile electron in a plane electromagnetic wave with peak amplitude of a_0: $\varepsilon_{\mathrm{vac}} \equiv \gamma_{\mathrm{vac}} m_e c^2$, where $\gamma_{\mathrm{vac}} \equiv 1 + a_0^2/2$. The observed energy increase is a clear advantage of using the hollow-core target instead of employing a pure vacuum setup.

Tracking of the injected electrons has revealed a significant difference in trajectories between TDA and LDA electrons. A vast majority of TDA electrons perform transverse oscillations across the channel that are characterized by crossing its axis ($y = 0$). Figure 3(d) quantifies the fraction of the TDA electrons that have crossed the axis as a function of the electron energy. Examples of these trajectories are shown in figure 3(b), where the blue-green color-scheme indicates the relativistic γ-factor along the trajectory. In contrast to the TDA electrons, the majority of the energetic LDA electrons never cross the axis of the channel. These are the electrons with energies above $500 m_e c^2$ in figure 3(d). The energetic LDA electrons remain relatively close to the wall. The corresponding trajectories are shown in figure 3(b) using the red-yellow color-scheme, where the color indicates the relativistic γ-factor along the trajectory.

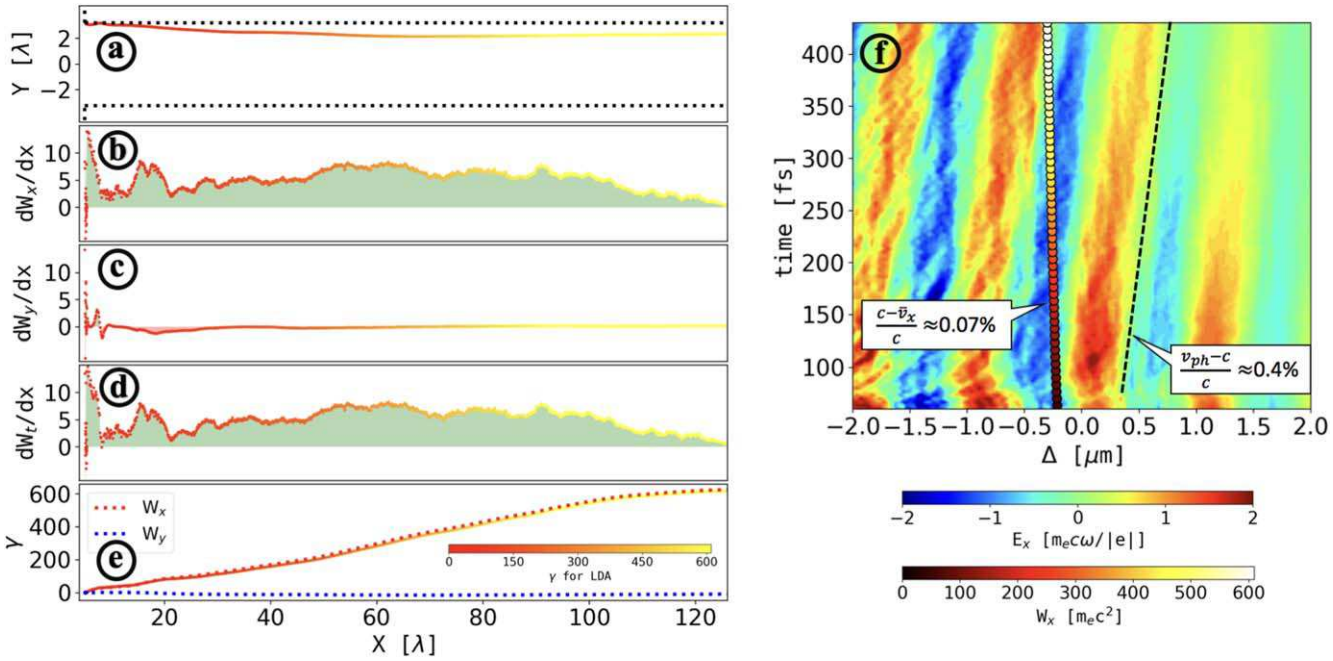

Figure 4. Detailed tracking information for a representative energetic LDA electron. The color-coding along the curves in panels (a)–(e) is the relativistic γ-factor. The quantities $\mathrm{d}W_{x,y,t}/\mathrm{d}x$ are normalized to $m_e\,c^2/\lambda$. The electron trajectory in panel (f) is plotted on top of the longitudinal electric field in a window moving forward with a speed of light, $\Delta \equiv x - ct - 12\lambda$. The color-coding of the markers indicates the work W_x performed by E_x.

The described qualitative differences in the trajectories are directly related to the key features in the two acceleration mechanisms. In what follows, we elucidate this aspect by tracking two representative electrons: one energetic LDA electron with $\max\gamma \approx 600$ that never crosses the axis of the channel and one energetic TDA electron with $\max\gamma \approx 400$ that performs a full oscillation across the channel.

Figure 4 provides detailed information about a selected LDA electron. As evident from the electron trajectory in figure 4(a), the longitudinal motion in the forward direction dominates. It is instructive to examine how the work performed by E_x and E_y changes as the electron moves along the channel. In order to do that, we plot $\mathrm{d}W_x/\mathrm{d}x$ (figure 4(b)) and $\mathrm{d}W_y/\mathrm{d}x$ (figure 4(c)) instead of plotting the accumulated quantities W_x and W_y. Figure 4(d) shows the change in the total work, $W_t \equiv W_x + W_y$. The accumulated area under this curve gives the relativistic γ-factor (or the electron energy) plotted in figure 4(e).

There are two aspects that are evident from figures 4(e) and (b): the electron energy comes predominantly from the work done by E_x, whereas the contribution of E_y is negligible; the electron continuously gains energy from E_x as it travels more than a hundred wavelengths along the channel. The influence of E_y is reduced because the transverse component of the electron velocity is relatively small compared to the longitudinal component. The continuous positive work by E_x suggests that the electron is moving sufficiently fast to remain in the accelerating part of the wave. This is further confirmed by figure 4(f), where E_x and the electron longitudinal location are plotted in a window moving with the speed of light, such that $\Delta \equiv x - ct - 12\lambda$. The electron indeed remains in the region with negative E_x over hundreds of fs, which allows it to efficiently gain energy.

Clearly, the key to achieving LDA is to ensure that an electron remains locked in an accelerating phase of the negative longitudinal electric field for an extended period of time. The reduction of the transverse force F_y^{HC} that we demonstrated in the previous section is critical: the transverse velocity remains small during the acceleration process, with the angle θ between $\mathbf{v}$ and the x-axis less than 2°. As a result, the average longitudinal electron velocity $\bar{v}_x$ is less than c by only 0.07%. In fact, the difference between the phase velocity of the wave, v_{ph}, and the speed of light is greater than $c - \bar{v}_x$. Indeed, we find that $c - \bar{v}_x \approx 7 \times 10^{-4}c$, whereas $v_{\mathrm{ph}} - c \approx 4 \times 10^{-3}\,c$. This means that the energy gain in our case is limited by the super-luminosity of the wave-fronts and not by the transverse or longitudinal electron motion.

In contrast to the considered LDA electron, a selected TDA electron whose detailed tracking information is shown in figure 5 has a relatively large initial transverse velocity v_y that was acquired at the injection stage. In this case, the angle between $\mathbf{v}$ and the x-axis is $\theta \approx 7°$. This allows the electron to traverse the channel while moving forward, as can be seen in figure 5(a), which, in turn, impacts the work done by E_x. The longitudinal laser electric field E_x is essentially an odd function of y, i.e. $E_x(y) \approx -E_x(-(y))$. This means that the electron switches between accelerating and decelerating regions by crossing the axis of the channel even if it has a sufficiently high longitudinal velocity to remain in the accelerating phase of the laser field for an extended period of time. This effect is well-illustrated in figures 5(a) and (b), where A and C mark the crossings of the channel axis. The work by E_x changes its sign not only at A and C, but also at D and E where the

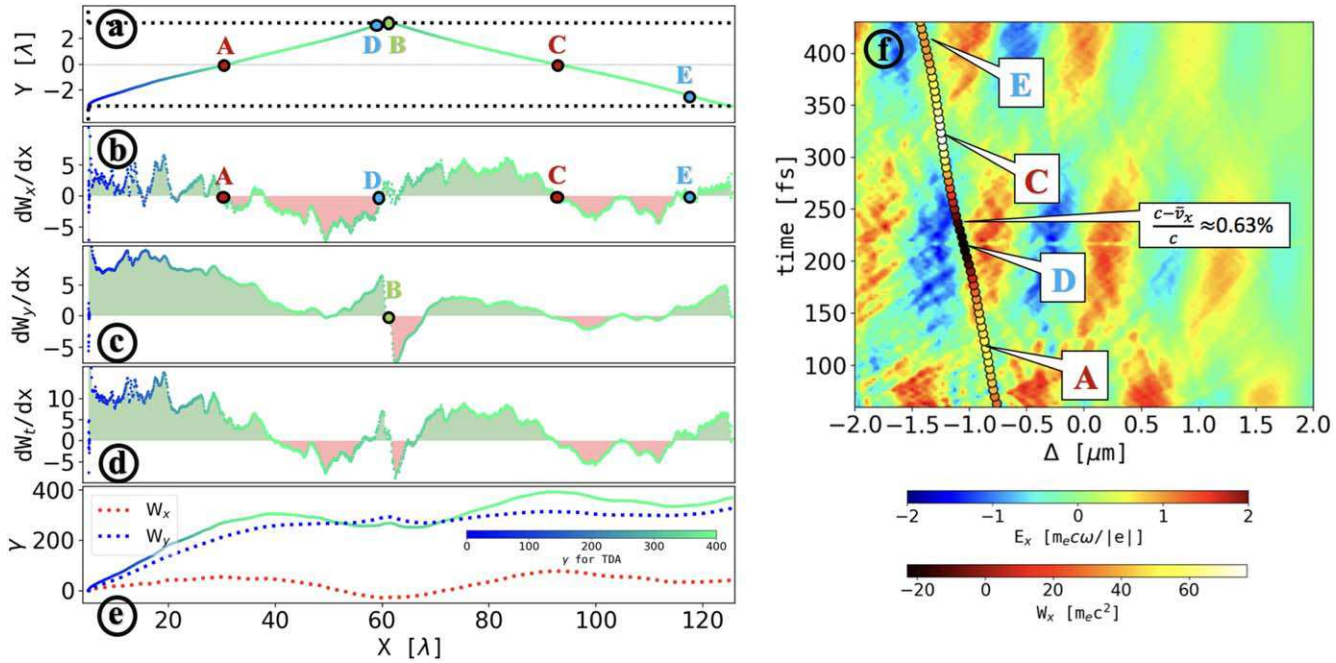

Figure 5. Detailed tracking information for a representative energetic TDA electron. The color-coding along the curves in panels (a)–(e) is the relativistic γ-factor. The quantities $dW_{x,y,t}/dx$ are normalized to $m_e\, c^2/\lambda$. The electron trajectory in panel (f) is plotted on top of the longitudinal electric field in a window moving forward with a speed of light, $\Delta \equiv x - ct - 12\ \lambda$. The color-coding of the markers indicates the work W_x performed by E_x.

electron slides out of the decelerating or accelerating phase due to its relative longitudinal motion with respect to the laser wave-fronts. The frequent alternations between the positive and negative work performed by E_x significantly reduce the electron energy gain from longitudinal laser electric field.

Most of the energy for the considered TDA electron comes from the transverse laser electric field (see figure 5(e)), which is the conventional DLA mechanism. Electron reflections off the channel walls (a reflection point is marked with a B) can aid the energy exchange between the electron and the transverse laser electric field E_y by changing the direction of v_y. As v_y flips, the compensation that usually exists between energy gain and loss in a purely vacuum case is disrupted. This can potentially lead to an appreciable energy increase, but this approach requires multiple bounces across the channel. It is worth pointing out that $c - \bar{v}_x \approx 6 \times 10^{-3} c$ is comparable to $v_{\rm ph} - c \approx 4 \times 10^{-3} c$, so the super-luminosity is not a major factor limiting the energy gain for the considered electron.

5. Collimated energetic electrons

In section 4, we examined how transverse and longitudinal laser electric fields contribute to acceleration of the injected electrons in the channel of a hollow-core target. In what follows, we examine the angular distribution of these electrons and how the two groups of electrons, LDA and TDA, contribute to it.

Figure 6(a) is the same scatter-plot of the accelerated electrons in the (W_x, W_y)-space as figure 3(c), but the color-coding now indicates the polar angle θ between the electron momentum and the axis of the channel. In order to generate this plot, we selected all macro-particles that are inside the channel, $|y| < 3.2\ \mu$m, after 400 fs into the simulation. The angle is then calculated by computing $\theta = \arctan(p_y/p_x)$ for each macroparticle, where p_x and p_y are the momentum components provided by the simulation. Electrons with a small angle θ are tightly clustered around $W_y = 0$ in figure 6(a), which suggests that that the LDA tends to produce well-collimated energetic electrons, but the transverse acceleration (TDA) does not.

As evident from figure 6(a), energetic TDA electrons have a polar angle whose absolute value exceeds 3°, while some fraction of the highly collimated energetic LDA electrons have a polar angle $|\theta| < 1°$. In order to gain more insight about the angular distribution of the energetic electrons, we plotted them in the (θ, γ)-space, with the scatter-plots for LDA and TDA electrons shown in figures 6(b) and (c). The curves in figure 6(d) show the total angular electron distribution and the corresponding contributions from LDA and TDA electrons that represent the scatter-plots from figures 6(b) and (c). The angular distribution of the TDA electrons has two symmetric peaks at $\theta \approx \pm 5°$. In contrast to that, the angular distribution of LDA electrons has a single sharp peak at $\theta \approx 0°$ with a full width half maximum of approximately 4°.

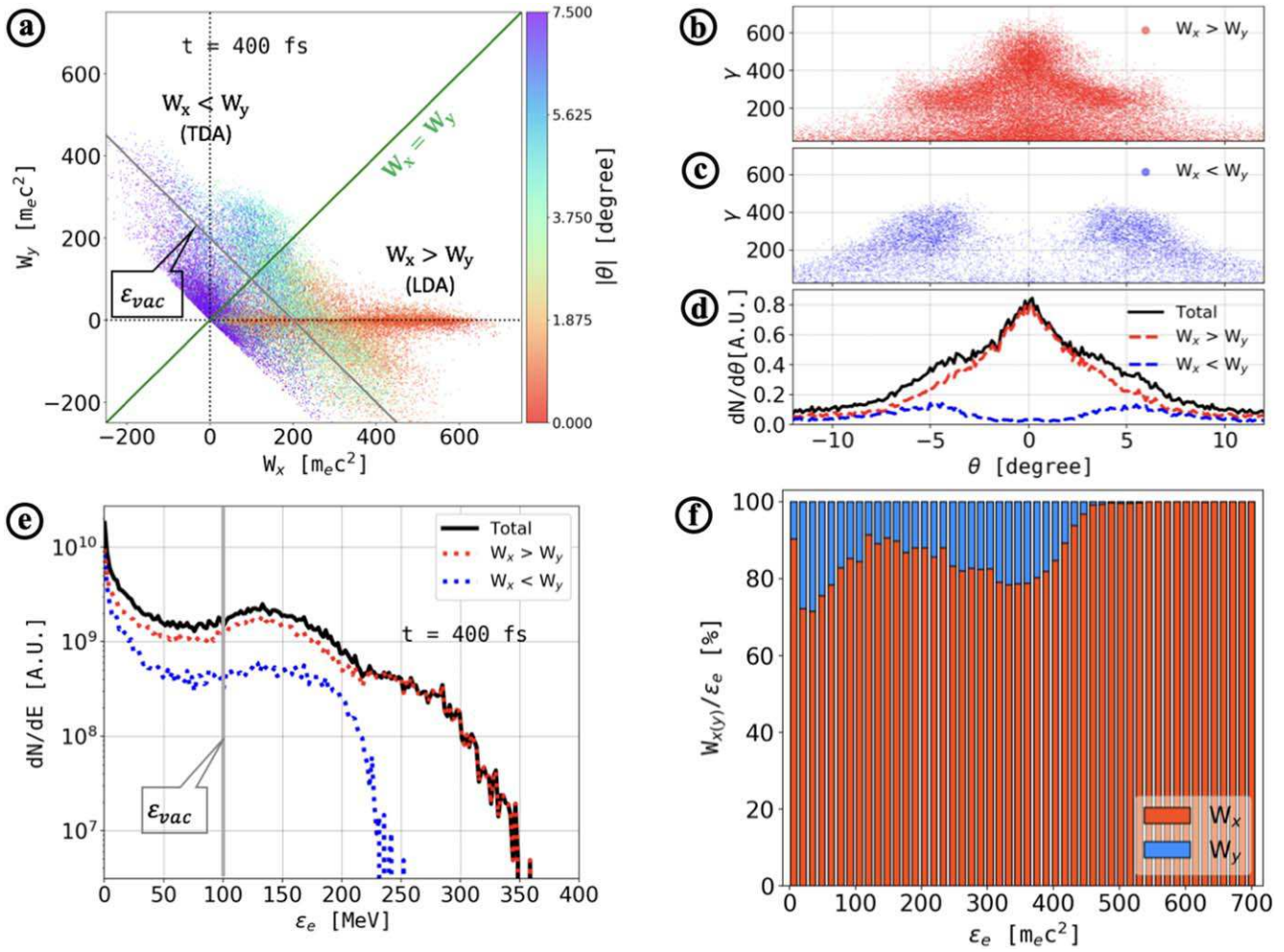

Figure 6. Angular distribution of accelerated electrons and their energy spectra. (a) The work performed by E_x and E_y on injected electrons over 400 fs is presented as a scatter-plot, with the color indicating the angle between the electron momentum and the x-axis. (b) and (c) LDA and TDA electrons are presented as scatter-plots in the (θ, γ)-space. (d) The angular distributions represent the scatter-plots shown in panels (b) and (c). (e) Energy spectra of injected electrons are shown after 400 fs. The spectra of LDA and TDA electrons are shown in red and blue. (f) The relative fraction of the energy contributed by E_x and E_y is shown as a function of the electron energy ε_e. These values are averaged over all injected electrons in a given energy bin.

The difference in the angular spread between the TDA and LDA electrons is determined by the transverse electron velocity gained during their injection into the channel. However, a detailed study of the injection dynamics and the factors determining the injection velocity goes beyond the scope of the current work. It is worth pointing out that although the angular spread of the TDA electrons is worse than that of the LDA electrons, it is still significantly better than the angular spread during the conventional DLA regime because of the reduced net restoring force inside the hollow channel.

The energy spectra of LDA and TDA electrons at $t = 400$ fs are shown in figure 6(e). The LDA electrons have a much higher cutoff energy (350 MeV) than the TDA electrons (250 MeV), but both energies significantly exceed $\varepsilon_{\rm vac} \approx 100$ MeV. The so-called super-ponderomotive part of the spectrum ($\varepsilon_e > \varepsilon_{\rm vac}$) is rather flat as compared to an exponentially decaying spectrum generated in a uniform target with the help of the conventional DLA (for example, see figure 5 in [12]). The longitudinal laser electric field E_x does most of the work over the entire range of electron energies, as can be seen in figure 6(f). This figure provides a relative fraction of the energy contributed by E_x and E_y, i.e. W_x/ε_e and W_y/ε_e, for electrons in a given energy bin.

Even though the emphasis has been on the longitudinal laser electric field, both components of the laser field are critical for producing energetic electrons with $\varepsilon_e > \varepsilon_{\rm vac}$ in a hollow-core target. We demonstrate this by performing an additional simulation where the polarization of the laser electric field is rotated by $\pi/2$ in the (y, z)-plane. In this case, there is no transverse laser electric field that is normal to the channel boundary. As a consequence, the electron injection into the channel is severely suppressed. Moreover, there is no strong longitudinal laser electric field, because the condition $\nabla \cdot E = 0$ can be satisfied for the transverse component E_z without any significant E_x. As a result, the maximum electron energy in this case is around 4 MeV.

6. Summary and discussion

In summary, we have demonstrated the importance of collective plasma effects in a hollow-core target for achieving

collimation of injected electrons that then enables the enhanced energy absorption from the longitudinal field of the laser. Using particle tracking, we have provided direct evidence that the superluminal phase velocity is the primary factor limiting the energy gain of the collimated electrons. We have also conclusively demonstrated that there is a direct correlation between θ and $W_\perp/W_\parallel$, such that a reduction in the contribution by the transverse laser field equates to a reduced divergence angle for the electrons.

The substantial angular divergence of electron beams produced by DLA is often considered as an inherent negative feature of the mechanism. The divergence however arises primarily because the standard approach relies on transverse electron oscillations and their interplay with the transverse electric fields of the laser pulse. Our approach is conceptually different, as it directly leverages longitudinal laser electric fields that are present in a tightly focused laser beam. Transverse oscillations that mediate the energy transfer between the laser pulse and the electrons in the traditional approach are no longer required.

In our scheme, transverse electron oscillations are reduced by creating a negatively charged electron channel, as opposed to a positively charged channel that is essential for the traditional DLA approach. Electrons are injected by the transverse laser electric field into the channel and then they are accelerated forward by the pulse, creating an electron current. The forces from electric and magnetic fields of this electron population compensate each other, creating a favorable configuration without a strong restoring force. Even though we use a trapezoidal temporal pulse profile in our manuscript to simplify the force analysis of section 3, the collimation mechanism is not sensitive to the shape of the laser pulse. PIC simulations for a 20 fs long Gaussian laser pulse yield results similar to those shown in figure 6.

Our 2D PIC simulations confirm that a highly directed electron beam with a low angular spread is produced due to a combination of the enhancement of the longitudinal laser field and the elimination of transverse oscillations. The electron cut-off energy of 350 MeV is much greater than the vacuum limit of $\varepsilon_{\rm vac} = (1 + a_0^2/2)m_e c^2 \approx 100$ MeV. Meanwhile, unlike the conventional DLA electron beam with a typical opening angle of 20°, our electron beam has an opening angle of less than 5°. The hollow-core target is essential for enhancing the longitudinal fields and maintaining them over a distance much longer than the Rayleigh length by guiding the laser pulse.

The key feature of our regime is that most of the energy (across the entire spectrum) is transferred to the electrons by the longitudinal laser electric field and, given a sufficient acceleration distance, super-ponderomotive energies can be realized without sacrificing the collimation. We speculatively suggest that this mechanism may have played a role in previous studies focused on high-energy laser-driven photon sources [31, 32], although further work is required to determine if such a connection exists. It also remains to be understood if the same mechanism can be realized by utilizing a microwire array [24, 25]. Previous results [24, 25] showed a well-collimated electron beam, but no super-ponderomotive electrons. We speculate that this might be a consequence of a relatively short acceleration length allowed to the electrons.

Further computational research is also required to determine how the described scenario scales with laser amplitude. The number of injected electrons is expected to increase with laser amplitude, which would lead to an increase of the transverse and longitudinal electric fields generated by the electrons. In appendix B, we estimate the strength of these electric fields. We find that the longitudinal field of an ultra-relativistic electron bunch remains small compared to the longitudinal electric field of the laser pulse, with the corresponding criterion given by equation (20). However, the impact of the quasi-static transverse electric field may not be always ignorable. This field is directed towards the axis of the channel, causing the ions to accelerate inwards. The inward ion motion leads to charge compensation in the channel. This reduces the transverse quasi-static electric field, while the quasi-static magnetic field remains unaffected. The described mechanism of electron collimation relies on a compensation between the forces of the quasi-static electric and magnetic field, but such a compensation is no longer possible after the ions fill up the channel and reduce the transverse electric field. We did check that the ion motion can be disregarded at the wave amplitude considered in our manuscript ($a_0 = 20$).

Acknowledgments

The work was supported by the National Basic Research Program of China (Grant No.2013CBA01502), NSFC (Grant Nos.11535001), National Grand Instrument Project (2012YQ030142), and the National Science Foundation (Grant No. 1632777). Simulations were performed using the EPOCH code (developed under UK EPSRC Grants No. EP/G054940/1, No. EP/G055165/1, and No. EP/G056803/1) using HPC resources provided by the TACC at the University of Texas. We appreciate the data collaboration supported by the SeedMe2 project (http://dibbs.seedme.org) [33].

Appendix A. PIC simulation parameters

All simulations presented in this work are 2D. They were carried out using a fully relativistic particle-in-cell code EPOCH [34]. For all but one simulation, the simulation box is a rectangle in the (x, y)-plane that is 130λ long ($0 \leqslant x \leqslant 130\lambda$) and 24λ wide ($-12\lambda \leqslant y \leqslant 12\lambda$). Here our grid size is $\Delta x = 1/50\lambda$ along the x-axis and $\Delta y = 1/20\lambda$ along the y-axis. In the simulation shown in figure 1, we used a wider box that is 48λ to perform the comparison of laser diffraction between the vacuum and the channel cases (the resolution is the same).

The laser pulse enters the domain at $x = 0$. It is a Gaussian beam in y with an axis at $y = 0$ and a focal plane at $x = 5$ μm. The laser wavelength is $\lambda = 1$ μm. In the vacuum case, the peak intensity is $I_0 = 5.4 \times 10^{20}$ W cm^{-2}, corresponding to $a_0 \approx 20$. The pulse has a trapezoid temporal

profile with 8.33 fs up/down ramps (2.5 laser periods each) and an 83.3 fs flattop (25 laser periods). We use open boundary conditions for the fields [34].

The structured target is initialized as a fully ionized uniform plasma slab ($5\ \mu\text{m} \leqslant x \leqslant 130\ \mu\text{m}$) with a hollow core ($|y| \leqslant 3.2\ \mu\text{m}$). The slab electron density is $n_e = 50n_c$ and it is initialized using 50 macro-particles per cell representing electrons. The ions are fully ionized carbon ions. Initially, their density is equal to $n_i = n_e/6$ and it is initialized using 25 macro-particles per cell representing ions. The ions are treated as immobile in our simulations to clearly distinguish the effect of the electron dynamics. The simulation with a uniform target uses a similar setup. In this case, the electron density is $n_e = 0.5n_c$, there is no channel, and the ion density is initialized using 10 macro-articles per cell.

It has been previously shown that the temporal resolution is critical for obtaining the correct electron energies during simulations of the DLA [35]. The criterion can be reformulated as $\Delta x \leqslant \lambda/a_0$ for $\Delta t \approx \Delta x/c$. To ensure the validity of our results, an extra simulation was performed with $\Delta x = 1/100\lambda$ and $\Delta y = 1/50\lambda$. The resulting electron energy spectra and electron angular divergence showed no significant change compared to those discussed in the manuscript. In order to aid the particle tracking process by reducing the data set, we used the resolution with $\Delta x = 1/50\lambda$ and $\Delta y = 1/20\lambda$.

Appendix B. Estimation of the longitudinal electric field generated by injected electrons

In our qualitative analysis, we have assumed that the longitudinal electric field generated by the injected negative charge is weak compared to the longitudinal field of the laser pulse. In what follows, we estimate this field to provide a criterion for when this assumption is valid.

Each electron bunch generates its own longitudinal electric field and the fields from different bunches can also add up to generate an even stronger longitudinal electric field. This collective field has to be relatively small. If this is the case, then, automatically, the field from an individual bunch is also small. This is the reason why we first focus our analysis on the collective field and then discuss the field of an individual bunch (see the end of the section).

In order to assess the the longitudinal electric field generated by the injected electrons, we consider a simple model where the injected electrons are approximated by a uniform cylinder that is moving along the channel with a given longitudinal relativistic velocity v. As shown in figure B1(b), the electron density, $n_e = n_0$, and the length of the cylinder, $L = L_0$, are given in the laboratory frame of reference S. It is convenient to characterize the longitudinal motion using the corresponding relativistic factor $\gamma = (1 - v^2/c^2)^{-1/2}$.

The electric field is easily calculated in a co-moving frame S' where the electrons are immobile because in this case the field is electrostatic. The collective field is the strongest at the ends of the cylinder. Assuming that $L' \gg R$, we immediately find that the longitudinal field is roughly given by

$$E'_{\parallel} \approx -|e|n'_e R \approx -|e|n_0 R/\gamma. \tag{13}$$

We took into account that the electrons whose longitudinal distance from the edge is much greater than R contribute very little to to total field, so the field is effectively generated by electrons in a volume of R^3. The transverse field in the co-moving frame is generated by the same limited volume of electrons, so this field is roughly equal to $E'_{\parallel}$ at the edge of the cylinder:

$$E'_{\perp} \approx E'_{\parallel} \approx -|e|n_0 R/\gamma. \tag{14}$$

The fields in the laboratory frame of reference are obtained via the Lorentz transformation, which yields

$$E_{\parallel} = E'_{\parallel} \approx -|e|n_0 R/\gamma, \tag{15}$$

$$E_{\perp} = \gamma E'_{\perp} \approx -|e|n_0 R. \tag{16}$$

We find that the longitudinal field in the laboratory frame S is reduced by a factor of γ compared to the transverse electric field. The estimate is based on the assumption that the electrons are highly relativistic, such that $L' = \gamma L_0 \gg R$ or, equivalently

$$\gamma \gg R/L_0. \tag{17}$$

This condition is satisfied in our simulations with a significant margin, as evident from figure B1(a).

Our last step is to compare the longitudinal field generated by the electrons to the longitudinal field of the laser pulse that can be estimated as

$$E_{\parallel}^{\text{laser}} \approx E_0 \lambda/R, \tag{18}$$

where we assume that the radius of the channel guiding the laser pulse with a transverse electric field amplitude of E_0 is roughly the same as the radius of the electron bunch. According to equations (15) and (16), the longitudinal field generated by the injected electrons is $E_{\parallel}^{\text{injected}} \approx E_{\perp}/\gamma$, where $E_{\perp}$ is the transverse field generated by the injected electrons. No electron injected by the laser field is possible if $E_{\perp} \gg E_0$, because the charge of the electrons that are already in the channel would prevent new electrons from being injected. Therefore, the upper estimate for the perpendicular field of the injected electrons is $E_{\perp} \approx E_0$. We then use this relation to find that

$$\frac{E_{\parallel}^{\text{injected}}}{E_{\parallel}^{\text{laser}}} \approx \frac{R}{\lambda\gamma}. \tag{19}$$

We thus conclude that the field of the injected electron has a relatively minor impact on their longitudinal motion if

$$R/\lambda \ll \gamma. \tag{20}$$

In our simulations, this condition is satisfied with a good margin as well. As evident from figure B1(a), we have $R/\lambda \approx 5$, whereas the typical value of the relativistic factor is $\gamma \approx 200$.

There are two points that need to be clarified regarding the provided estimate for the longitudinal electric field. Our estimate neglects the positive charge that is generated in the walls of the channel. Its presence is evident in figure B1(a), where the red color shows the positive charge density. The

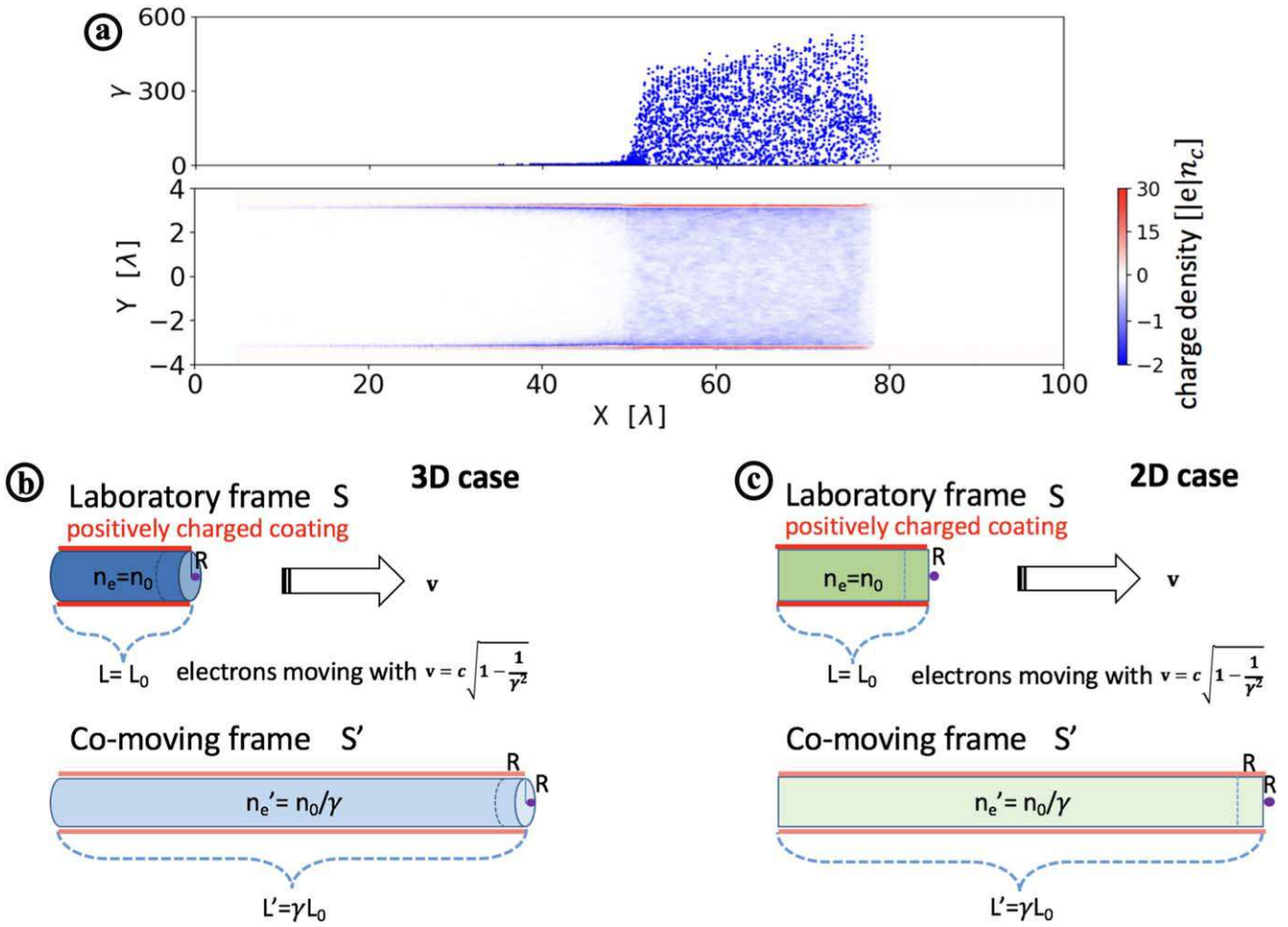

Figure B1. A cloud of injected electrons moving along the hollow-core of the target. (a) Snapshots from the PIC simulation taken at $t = 266$ fs. The upper panel is a scatter plot of the relativistic γ-factor in the electron cloud, whereas the lower panel is the charge density, normalized to $|e|n_c$, in the vicinity of the cloud. (b) and (c) Simple models for the electron cloud that are used to estimate transverse and longitudinal electric fields. In 3D, the cloud is a uniform cylinder with positively charged coating. In 2D, the cloud is a uniform rectangle with positively charged edges.

positive charge trails the injected electron bunch. This positive 'coating' generates a field that counteracts the field generated by the injected electrons. This compensation becomes significant inside the electron cloud. Therefore, our estimate can be viewed as the 'worst case scenario'. Our estimate is performed for an electron cylinder, which means that the estimate is performed in 3D. Our simulation is performed in 2D, so the estimates need to be adjusted accordingly. However, the main result given by equation (19) remains unchanged. The field compensation provided by the positive 'coating' becomes much more important in 2D because of the divergent nature of the electrostatic potential at large distances.

In our analysis, we have considered the entire population of the injected electrons, but a similar analysis would apply for each of the electron bunches. The length of each bunch is roughly half the wavelength, $L_0 \approx 0.5$ μm, so it satisfies the condition given by equation (17). The important conclusion that follows is that separate bunches effectively do not interact in our case. The longitudinal field of a single bunch is reduced by a factor of γ so its own longitudinal field is relatively small and can be neglected, provided that the condition (20) is satisfied. It should be noted that γ may not be sufficiently high right after the electron injection, so the longitudinal field of the injected bunch may impact the electron dynamics at that early stage of the acceleration.

ORCID iDs

Z Gong https://orcid.org/0000-0002-6272-1853
A P L Robinson https://orcid.org/0000-0002-3967-7647
A V Arefiev https://orcid.org/0000-0002-0597-0976

References

[1] Strickland D and Mourou G 1985 Compression of amplified chirped optical pulses *Opt. Commun.* **55** 447–9
[2] Mourou G A, Korn G, Sandner W and Collier J L 2011 *ELI-Extreme Light Infrastructure: Science and Technology with Ultra-Intense Lasers, Whitebook* (Berlin: THOSS Media GmbH)

[3] Danson C, Hillier D, Hopps N and Neely D 2015 Petawatt class lasers worldwide *High Power Laser Sci. Eng.* **3** E3

[4] Pukhov A, Sheng Z-M and Meyer-ter Vehn J 1999 Particle acceleration in relativistic laser channels *Phys. Plasmas* **6** 2847–54

[5] Gahn C, Tsakiris G, Pukhov A, Meyer-ter Vehn J, Pretzler G, Thirolf P, Habs D and Witte K 1999 Multi-mev electron beam generation by direct laser acceleration in high-density plasma channels *Phys. Rev. Lett.* **83** 4772

[6] Gibbon P 2004 *Short Pulse Laser Interactions with Matter* (Singapore: World Scientific)

[7] Svelto O and Hanna D C 1998 *Principles of Lasers* (Berlin: Springer)

[8] Stupakov G V and Zolotorev M 2001 Ponderomotive laser acceleration and focusing in vacuum for generation of attosecond electron bunches *Phys. Rev. Lett.* **86** 5274

[9] Robinson A and Arefiev A 2018 Interaction of an electron with coherent dipole radiation: role of convergence and anti-dephasing *Phys. Plasmas* **25** 053107

[10] Max C E, Arons J and Langdon A B 1974 Self-modulation and self-focusing of electromagnetic waves in plasmas *Phys. Rev. Lett.* **33** 209

[11] Wang H, Lin C, Sheng Z, Liu B, Zhao S, Guo Z, Lu Y, He X, Chen J and Yan X 2011 Laser shaping of a relativistic intense, short gaussian pulse by a plasma lens *Phys. Rev. Lett.* **107** 265002

[12] Arefiev A, Khudik V, Robinson A, Shvets G, Willingale L and Schollmeier M 2016 Beyond the ponderomotive limit: Direct laser acceleration of relativistic electrons in sub-critical plasmas *Phys. Plasmas* **23** 056704

[13] Pukhov A 2002 Strong field interaction of laser radiation *Rep. Prog. Phys.* **66** 47

[14] Arefiev A V, Breizman B N, Schollmeier M and Khudik V N 2012 Parametric amplification of laser-driven electron acceleration in underdense plasma *Phys. Rev. Lett.* **108** 145004

[15] Khudik V, Arefiev A, Zhang X and Shvets G 2016 Universal scalings for laser acceleration of electrons in ion channels *Phys. Plasmas* **23** 103108

[16] Liu B, Wang H, Liu J, Fu L, Xu Y, Yan X and He X 2013 Generating overcritical dense relativistic electron beams via self-matching resonance acceleration *Phys. Rev. Lett.* **110** 045002

[17] Hu R, Liu B, Lu H, Zhou M, Lin C, Sheng Z, Chen C-E, He X and Yan X 2015 Dense helical electron bunch generation in near-critical density plasmas with ultrarelativistic laser intensities *Sci. Rep.* **5** 15499

[18] Ji L, Pukhov A, Kostyukov I Y, Shen B and Akli K 2014 Radiation-reaction trapping of electrons in extreme laser fields *Phys. Rev. Lett.* **112** 145003

[19] Ji L, Pukhov A, Nerush E, Kostyukov I Y, Shen B and Akli K 2014 Energy partition, γ-ray emission, and radiation reaction in the near-quantum electrodynamical regime of laser-plasma interaction *Phys. Plasmas* **21** 023109

[20] Liu B, Hu R, Wang H, Wu D, Liu J, Chen C, Meyer-ter Vehn J, Yan X and He X 2015 Quasimonoenergetic electron beam and brilliant gamma-ray radiation generated from near critical density plasma due to relativistic resonant phase locking *Phys. Plasmas* **22** 080704

[21] Stark D, Toncian T and Arefiev A 2016 Enhanced multi-mev photon emission by a laser-driven electron beam in a self-generated magnetic field *Phys. Rev. Lett.* **116** 185003

[22] Chang H, Qiao B, Huang T, Xu Z, Zhou C, Gu Y, Yan X, Zepf M and He X 2017 Brilliant petawatt gamma-ray pulse generation in quantum electrodynamic laser-plasma interaction *Sci. Rep.* **7** 45031

[23] Gong Z, Hu R H, Lu H Y, Yu J Q, Wang D H, Fu E G, Chen C E, He X T and Yan X Q 2018 Brilliant gev gamma-ray flash from inverse compton scattering in the qed regime *Plasma Phys. Control. Fusion* **60** 044004

[24] Jiang S, Krygier A, Schumacher D, Akli K and Freeman R 2014 Effects of front-surface target structures on properties of relativistic laser-plasma electrons *Phys. Rev.* E **89** 013106

[25] Jiang S *et al* 2016 Microengineering laser plasma interactions at relativistic intensities *Phys. Rev. Lett.* **116** 085002

[26] Xiao K *et al* 2016 Energetic electron-bunch generation in a phase-locked longitudinal laser electric field *Phys. Rev.* E **93** 043207

[27] Naumova N, Sokolov I, Nees J, Maksimchuk A, Yanovsky V and Mourou G 2004 Attosecond electron bunches *Phys. Rev. Lett.* **93** 195003

[28] Kluge T *et al* 2012 High proton energies from cone targets: electron acceleration mechanisms *New J. Phys.* **14** 023038

[29] Zou D, Pukhov A, Yi L, Zhuo H, Yu T, Yin Y and Shao F 2017 Laser-driven ion acceleration from plasma micro-channel targets *Sci. Rep.* **7** 42666

[30] Ji L, Snyder J, Pukhov A, Freeman R and Akli K 2016 Towards manipulating relativistic laser pulses with micro-tube plasma lenses *Sci. Rep.* **6** 23256

[31] Yi L, Pukhov A, Luu-Thanh P and Shen B 2016 Bright x-ray source from a laser-driven microplasma waveguide *Phys. Rev. Lett.* **116** 115001

[32] Yu J, Hu R, Gong Z, Ting A, Najmudin Z, Wu D, Lu H, Ma W and Yan X 2018 The generation of collimated γ-ray pulse from the interaction between 10 pw laser and a narrow tube target *Appl. Phys. Lett.* **112** 204103

[33] Chourasia A, Nadeau D and Norman M 2017 Seedme: data sharing building blocks *Proc. Practice and Experience in Advanced Research Computing 2017 on Sustainability, Success and Impact PEARC17 (New York)* (ACM) p 69:1

[34] Arber T *et al* 2015 Contemporary particle-in-cell approach to laser-plasma modelling *Plasma Phys. Control. Fusion* **57** 113001

[35] Arefiev A V, Cochran G E, Schumacher D W, Robinson A P and Chen G 2015 Temporal resolution criterion for correctly simulating relativistic electron motion in a high-intensity laser field *Phys. Plasmas* **22** 013103